Organometallic Synthesis of Colloidal α-/β-NiAl Nanoparticles and Selective Aluminum Oxidation in α-Ni$_{1-x}$Al$_x$ Nanoalloys

Mirza Cokoja,[†] Harish Parala,[†] Alexander Birkner,[‡] Osama Shekhah,[‡]
Maurits W. E. van den Berg,[§] and Roland A. Fischer*,[†]

Lehrstuhl für Anorganische Chemie II—Organometallics and Materials, Lehrstuhl für Physikalische Chemie I, and Lehrstuhl für Technische Chemie, Ruhr-Universität Bochum, Universitätsstrasse 150, D-44780 Bochum, Germany

A novel soft chemical synthesis of Ni$_{1-x}$Al$_x$ nanoparticles ($0.09 \leq x \leq 0.50$) by cohydrogenolysis of [Ni(cod)$_2$] (**1**) with [(AlCp*)$_4$] (**2**) or with [(Me$_3$N)AlH$_3$] (**3**) in nonaqueous solution is presented (cod = 1,5-cyclooctadiene, Cp* = 1,2,3,4,5-cyclopentadienyl). The treatment of equimolar amounts of **1** and **2** in mesitylene solution under 3 bar of H$_2$ at 150 °C gave a brown-black colloidal solution of intermetallic β-NiAl particles, characterized by transmission electron microscopy/energy dispersive X-ray analysis (TEM/EDX) and powder X-ray diffraction (XRD). The solution was stable under 3 bar of H$_2$ at 150 °C for up to 8 h. The β-NiAl colloids were treated postsynthesis with ^{17}O-enriched 1-adamantanecarboxylic acid (ACA) as a surface capping group, giving nearly monodisperse α-NiAl colloids that were stable under argon at room temperature for weeks. The coordination of ACA at the α-NiAl surface was studied by ^{17}O NMR and IR spectroscopy. A series of α-Ni$_{1-x}$Al$_x$ samples with a variety of compositions ($x =$ 0.50, 0.33, 0.25, 0.17, 0.09) were prepared analogously, and the samples were characterized by means of elemental analysis (ICP), XRD, and TEM/EDX. Air oxidation of α-Ni$_{1-x}$Al$_x$ nanoparticles leads to core−shell particles of the type (Al$_2$O$_3$)$_{\delta/2}$@Ni$_{1-x}$Al$_{x-\delta}$ ($0.09 \leq x \leq 0.50$; $x > \delta$). XRD, X-ray photoelectron spectroscopy (XPS), and X-ray absorption spectroscopy (XAS) analyses showed that the Ni core is protected against oxidation down to an Al content of about 10 atom %.

Introduction

The aluminides MAl of the late 3d metals Fe, Co, Ni, and Cu represent a series of binary intermetallic Hume−Rothery phases that are of special importance in material sciences.[1] Nickel aluminide, presumably the most prominent representative, is an attractive material for many industrial products, e.g., car and machine parts or turbine blades,[2] due to its bulk physical properties such as low density, high melting point, and creep resistance.[3] NiAl in particular exhibits excellent corrosion stability. The formation of a crystalline γ-Al$_2$O$_3$ layer on thin films of NiAl by preferential Al oxidation and the diffusion of Al onto the surface of NiAl phases upon oxidation were studied in detail.[4−6] But as well, nickel aluminide alloys play an important role in catalysis. For example, Raney nickel, which is the archetypical catalyst of olefin hydrogenation, is a nanoporous Ni material prepared from the NiAl alloy and formed by leaching of Al under basic conditions.[7]

The metallurgy and chemistry of ultrafine and nanocrystalline metal aluminide powders including the surface oxidation has more recently been studied largely because of improving the materials properties of aluminide-based alloys as the Hall−Petch effect predicts an increase of hardness or strength associated with decreasing grain size.[8] Nanoscale aluminide powder materials are typically prepared by metallurgical processes such as high-energy mechanical milling or welding,[9] arc plasma,[10] spray pyrolysis,[11] and laser evaporation/condensation.[12] Chemical approaches to microcrystalline NiAl powders include, for example, the report of Withers et al. on the reaction of NiCl$_2$ and Al at 750 °C in a molten eutectic salt mixture of NaCl and KCl.[13] Abe and Tsuge combined NiCl$_2$ and AlCl$_3$ in presence of ammonium

* To whom correspondence should be addressed. E-mail: roland.fischer@ruhr-uni-bochum.de. Tel.: (+49) 234-32-24174. Fax: (+49) 234-32-14174.
    † Lehrstuhl für Anorganische Chemie II—Organometallics and Materials.
    ‡ Lehrstuhl für Physikalische Chemie I.
    § Lehrstuhl für Technische Chemie.

(1) Sauthoff, G., Ed. *Intermetallics*; Wiley-VCH: Weinheim, Germany, 1995.
(2) (a) Rigney, J. D.; Scott, W. S.; Darolia, R.; Corderman, R. R. Eur. Pat. Appl. EP 0992612 A2, 2000. (b) Darolia, R. *JOM* **1991**, *43*, 44−49.
(3) (a) Jha, S. C.; Ray, R. *JOM* **1990**, *42*, 58−61. (b) Bonetti, E.; Campari, E. G.; Pasquini, L.; Sampaolesi, E.; Scipione, G. *Nanostruct. Mater.* **1999**, *12*, 895−898.
(4) (a) Jaeger, R. M.; Kuhlenbeck, H.; Freund, H.-J.; Wuttig, M.; Hoffmann, W.; Franchy, R.; Ibach, H. *Surf. Sci.* **1991**, *259*, 235−252. (b) Klimenkov, M.; Nepijko, S.; Kuhlenbeck, H.; Freund, H.-J. *Surf. Sci.* **1997**, *385*, 66−76. (c) Ceballos, G.; Song, Z.; Pascual, J. I.; Rust, H.-P.; Conrad, H.; Bäumer, M.; Freund, H.-J. *Chem. Phys. Lett.* **2002**, *359*, 41−47.

(5) (a) Brumm, M. W.; Grabke, H. J. *Corros. Sci.* **1992**, *33*, 1667−1675. (b) Brumm, M. W.; Grabke, H. J. *Corros. Sci.* **1993**, *34*, 547−553. (c) Brumm, M. W.; Grabke, H. J.; Wagemann, B. *Corros. Sci.* **1994**, *36*, 37−53. (d) Grabke, H. J.; Brumm, M. W.; Wagemann, B. *Mater. Corros.* **1996**, *47*, 675−677.
(6) (a) Bäumer, M.; Freund, H.-J. *Prog. Surf. Sci.* **1999**, *61*, 127−198. (b) Stierle, A.; Renner, F.; Streitel, R.; Dosch, H.; Drube, W.; Cowie, B. C. *Science* **2004**, *303*, 1652−1656. (c) Kresse, G.; Schmid, M.; Napetschnig, E.; Shishkin, M.; Köhler, L.; Varga, P. *Science* **2005**, *308*, 1440−1442.
(7) (a) Raney, M. U.S. Patent 1,628,190, 1927. (b) Fouilloux, P. *Appl. Catal.* **1983**, *8*, 1−42.
(8) Chen, T.; Hampikian, J. M.; Thadhani, N. N. *Acta Mater.* **1999**, *47*, 2567−2579.

carboxlyates; the subsequent annealing at 1400 °C gave a mixture of NiAl and Ni₃Al.[14] Alternative soft chemical strategies were developed in particular aiming at nanocrystalline aluminides, i.e., TiAl,[15] FeAl,[16] and NiAl.[17] One concept is based on the reaction of metal halides with lithium tetrahydridoaluminate in nonaqueous media which is thought to generate intermediate species such as $[M(AlH_4)_n]$ which are thermally labile and decompose into MAl at temperatures even below 200 °C. In particular, Buhro and co-workers reported on the reaction of $NiCl_2$ and $LiAlH_4$ in boiling mesitylene to yield a black, pyrophoric powder, which led to the desired NiAl phase upon annealing the obtained raw material at 550 °C.[17] Similarly, Tillement et al. claimed a successful wet chemical approach to NiAl powder by the reduction of $[Ni(OAc)_2]$ (Ac = CH_3CO) and $[Al(acac)_3]$ (acac = acetylacetonate) with an excess of NaH and traces of *tert*-butanol in boiling THF.[18] Finally, a halide- and oxo-ligand-free, fully *organometallic* synthesis of NiAl was presented by Bönnemann et al.[19] The reaction of $[Ni(cod)_2]$ (cod = 1,5-cyclooctadiene) with $AlEt_3$ in toluene under 50–100 bar of H_2 at room temperature gave an undefined black material, which was isolated as reaction intermediate, then treated with H_2 at 200 °C, and subsequently annealed in an argon stream at 300 °C to give a phase-pure NiAl powder with an average particle size of 2–4 nm. Looking through

these previous publications, there appears to be no serious claim on a straightforward, one-step wet chemical precursor route to nanocrystalline NiAl particles in solution to date, and consequently colloidal dispersions of free-standing NiAl nanoparticles in nonaqueous media are so far not accessible. Certainly, the hydrogenolysis of labile all-hydrocarbon organometallic precursors following the concepts of Bönnemann et al.[19] and Chaudret and co-workers[20] holds great promise for wet chemical nanometallurgy in general. However, the key for the wet chemical synthesis of metal aluminides in particular is obviously a good precursor for the Al component matching the precursor chemistry of the transition metal component. Recently, we introduced the low-valent aluminum organyl $[(AlCp^*)_4]$ as a novel source for aluminum. It quantitatively decomposes to Al nanoparticles under hydrogen at 150 °C with 1,2,3,4,5-pentamethylcyclopentadiene (Cp*H) as the only byproduct, whereas $AlEt_3$ is very stable at these conditions.[21] The cohydrogenolysis of $[CpCu(PMe_3)]$ with $[(AlCp^*)_4]$ in boiling mesitylene allowed the selective synthesis of the intermetallic compound θ-CuAl₂. In the presence of poly(2,6-dimethyl-1,4-phenylene oxide) (PPO), colloidal solutions of α-Cu$_{1-x}$Al$_x$ nanoparticles were prepared, too.[21] Similarly, we described the synthesis of α- and β-CuZn (brass) nanoparticles and colloids by cohydrogenolysis of $[CpCu(PMe_3)]$ with $[ZnCp^*_2]$.[22] The M–Cp* bond is comparably weak for late transition metals and main group metals. Hydrogenolysis yields Cp*H as a clean, chemically innocent leaving group.

Hence, our report below deals with the development of a novel, very clean organometallic route for the soft chemical synthesis of nickel aluminide nanoparticles stabilized as colloids in nonaqueous solution, with a free variation of the Al content in the sample. The complexes $[Ni(cod)_2]$, which is a well-known source for Ni(0),[23] and $[(AlCp^*)_4]$ were chosen as precursors. Also, we compared $[(AlCp^*)_4]$ with $[(Me_3N)AlH_3]$ as Al sources. In addition, a comprehensive study of the oxidation behavior of the nickel aluminide particles with decreasing the Al content, especially in Ni-rich α-NiAl phases, was performed.

Experimental Section

General Techniques of Sample Preparation. All manipulations and chemical reactions were conducted using Schlenk-line and glovebox techniques (Ar, H_2O, O_2 < 1 ppm) and sealed Fischer–Porter vessels (Andrews Glass, volume: 90 mL). Notably, the Si–OH surfaces of all glass vessels, including NMR tubes, were silylated using boiling hot 1,1,1,3,3,3-hexamethyldisilaazane (99%, Acros) prior to usage. Mesitylene and cyclohexene were dried by

(9) (a) Kiss, L. F.; Kaptás, D.; Balogh, J.; Bujdosó, L.; Kemény, T.; Vincze, I. *Phys. Status Solidi A* **2004**, *201*, 3333–3337. (b) Abbasi, M.; Taheri, A. K.; Salehi, M. T. *J. Alloys Compd.* **2001**, *319*, 233–241. (c) Xi, S.; Qu, X.; Ma, M.; Zhou, J.; Zheng, X.; Wang, X. *J. Alloys Compd.* **1998**, *268*, 211–214. (d) Huang, B.-L.; Lavernia, E. J. *J. Mater. Synth. Process.* **1995**, *3*, 1–10. (e) Suryanarayana, C.; Froes, F. H. *Mater. Sci. Eng., A* **1994**, *A179–A180*, 108–111. (f) Suryanarayana, C.; Froes, F. H. *Adv. Mater.* **1993**, *5*, 96–106. (g) Itsukaichi, T.; Masuyama, K.; Umemoto, M.; Okane, I.; Cabanas-Moreno, J. G. *J. Mater. Res.* **1993**, *8*, 1817–1828. (h) Jang, J. S. C.; Koch, C. C. *J. Mater. Res.* **1990**, *5*, 498–510.

(10) (a) Grin, Y.; Wagner, F. R.; Armbrüster, M.; Kohout, M.; Leithe-Jasper, A.; Schwarz, U.; Wedig, U.; von Schnering, H. G. *J. Solid State Chem.* **2006**, *179*, 1707–1719. (b) Wang, Z.; Fan, A. L.; Tian, W. H.; Wang, Y. T.; Li, X. G. *Mater. Lett.* **2006**, *60*, 2227–2231. (c) Havinga, E. E.; Damsma, H.; Hokkeling, P. *J. Less-Common Met.* **1972**, *27*, 169–186.

(11) (a) Geibel, A.; Froyen, L.; Delaey, L.; Leuven, K. U. *J. Therm. Spray Technol.* **1996**, *5*, 419–430. (b) Tsunekawa, Y.; Okumiya, M.; Gotoh, K.; Nakamura, T.; Niimi, I. *Mater. Sci. Eng., A* **1992**, *A159*, 253–259.

(12) (a) Pithawalla, Y. B.; El Shall, M. S.; Deevi, S. C. *Intermetallics* **2000**, *8*, 1225–1231. (b) Bohn, R.; Haubold, T.; Birriger, R.; Gleiter, H. *Scr. Metall. Mater.* **1990**, *25*, 811–816. (c) Haubold, T.; Bohn, R.; Birriger, R.; Gleiter, H. *Mater. Sci. Eng., A.* **1992**, *A153*, 679–683. (d) Chang, H.; Altstetter, C. J.; Averback, R. S. *J. Mater. Res.* **1992**, *7*, 2962–2970.

(13) Withers, J. C.; Shiao, H.-C.; Loutfy, R. O.; Wang, P. *JOM* **1991**, *43*, 36–39.

(14) Abe, O.; Tsuge, A. *J. Mater. Res.* **1991**, *6*, 928–934.

(15) Haber, J. A.; Crane, J. L.; Buhro, W. E.; Frey, C. A.; Sastry, S. M. L.; Balbach, J. J.; Conradi, M. S. *Adv. Mater.* **1996**, *8*, 163–166.

(16) (a) Pithawalla, Y. B.; Deevi, S. *Mater. Res. Bull.* **2004**, *39*, 2303–2316. (b) Dutta, D. P.; Sharma, G.; Rajarajan, A. K.; Yusuf, S. M.; Dey, G. K. *Chem. Mater.* **2007**, *19*, 1221–1225.

(17) (a) Buhro, W. E.; Haber, J. A.; Waller, B. E.; Trentler, T. J.; Suryanarayanan, R.; Frey, C. A.; Sastry, S. M. L. *Polym. Mater. Sci.* **1995**, *73*, 39–40. (b) Haber, J. A.; Gunda, N. V.; Buhro, W. E. *J. Aerosol Sci.* **1998**, *29*, 637–645. (c) Haber, J. A.; Gunda, N. V.; Balbach, J. J.; Conradi, M. S.; Buhro, W. E. *Chem. Mater.* **2000**, *12*, 973–982.

(18) Tillement, O.; Illy-Cherrey, S.; Dubois, J. M.; Bégin-Colin, S.; Massicot, F.; Schneider, R.; Fort, Y.; Ghanbaja, J.; Bellouard, C.; Belin-Ferré, E. *Philos. Mag. A* **2002**, *82*, 913–923.

(19) Bönnemann, H.; Brijoux, W.; Hofstadt, H.-W.; Ould-Ely, T.; Schmidt, W.; Wassmuth, B.; Weidenthaler, C. *Angew. Chem., Int. Ed.* **2002**, *41*, 599–603.

(20) (a) Dumestre, F.; Amiens, C.; Chaudret, B.; Renaud, P.; Fejes, P. *Science* **2004**, *303*, 821–823. (b) Dumestre, F.; Amiens, C.; Chaudret, B.; Respaud, M.; Fejes, P.; Renaud, P.; Zurcher, P. *Angew. Chem., Int. Ed.* **2003**, *42*, 5213–5216.

(21) Cokoja, M.; Parala, H.; Schröter, M.-K.; Birkner, A.; van den Berg, M. W. E.; Grünert, W.; Fischer, R. A. *Chem. Mater.* **2006**, *18*, 1634–1642.

(22) Cokoja, M.; Parala, H.; Schröter, M.-K.; van den Berg, M. W. E.; Klementiev, K. V.; Grünert, W.; Fischer, R. A. *J. Mater. Chem.* **2006**, *16*, 2420–2428.

(23) (a) Ould-Ely, T.; Amiens, C.; Chaudret, B.; Snoeck, E.; Verelst, M.; Respaud, M.; Broto, J.-M. *Chem. Mater.* **1999**, *11*, 526–529. (b) Cordente, N.; Respaud, M.; Senocq, F.; Casanove, M.-J.; Amiens, C.; Chaudret, B. *Nano Lett.* **2001**, *1*, 565–568.

passing through a Schlenk frit filled with dry, activated alumina (chromatography grade, Merck) and subsequent distillation. All other solvents used were dried, degassed, and argon-saturated by using a continuous solvent purification system (MBraun; H_2O content below 1 ppm). The precursors $[Ni(cod)_2]$[24] and $[(AlCp^*)_4]$[25] were synthesized according to the literature. $[(Me_3N)AlH_3]$ was prepared by a modification of the procedure published by Jouet et al.[26] The synthesis was carried out in toluene instead of diethyl ether, and the product was not sublimed but crystallized from a saturated toluene solution. [17]O-enriched water (enrichment grade 35−40%) was purchased from Deutero GmbH. 1-Adamantanecarbonyl chloride was purchased from Aldrich.

Elemental Analysis. The analysis for the metal content was undertaken using a Spectro Modula inductively coupled plasma (ICP) instrument. The C and H content was measured with an Elementar Vario III instrument.

NMR Spectroscopy. All high-resolution NMR spectra in solution were recorded on a Bruker DPX 250 spectrometer in C_6D_6 and mesitylene-d_{12} ($T = 25$ °C; ^{1}H, 250.1 MHz; ^{13}C, 62.9 MHz; [27]Al, 65.2 MHz; [17]O, 33.9 MHz). The chemical shifts (in δ ppm) are referenced to the residual proton signals of the deuterated solvent (C_6D_6: [1]H, 7.15 ppm; ^{13}C, 128 ppm. Mesitylene-d_{12}: [1]H, 6.67 and 2.13 ppm) or the probe head ([27]Al: 68.0 ppm, referenced to $[Al(H_2O)_6]^{3+}$ set at 0.0 ppm). In situ NMR reactions were done using pressure-stable NMR tubes with Young PTFE screw caps (Wilmad-LabGlass).

Infrared Spectroscopy. IR measurements (KBr pellets) were carried out on a Perkin-Elmer 1720 X Fourier transform spectrometer.

Gas Chromatography. GC−MS (gas chromatography−mass spectrometry) measurements were performed on a Shimadzu GCMS-QP2010 using standard settings for hydrocarbon separation.

X-ray Diffraction Studies. All powder X-ray diffractograms were recorded on a D8-Advance Bruker AXS diffractometer (Cu Kα radiation) in $\theta-2\theta$ geometry with a position-sensitive detector (capillary technique under argon, thickness: 0.7 mm).

Transmission Electron Microscopy. TEM measurements were carried out on a Hitachi H-8100 instrument (accelerating voltage up to 200 kV, LaB$_6$ filament). High-resolution transmission electron microscopy (HRTEM) studies were performed at the Hahn−Meitner Institute in Berlin on a Philips CM12 instrument with an accelerating voltage up to 120 kV. All TEM samples were prepared as diluted solutions or suspensions in toluene on carbon-coated copper or gold grids (Plano).

X-ray Photoelectron Spectra. X-ray photoelectron spectra (XPS) were recorded on a modified ultrahigh vacuum Leybold MAX system, equipped with an EA11 energy analyzer and an X-ray twin anode (Al Kα, Mg Kα). The measurements were undertaken using Al Kα radiation (1486.6 eV). The pass energy for the survey spectrum was set to 200 eV and for the region spectra to 46.1 eV. The spectra were calibrated to the O KLL edge (binding energy 978 eV).

X-ray Absorption Spectra. The absorption edge of Ni at 8333.0 eV was measured at Hasylab E4 station (Hamburg, Germany). This beamline was equipped with a Si(111) double-crystal monochromator that was used to detune to 50% of the maximum intensity in order to exclude higher harmonics present in the X-ray beam. Samples were mixed with cellulose and pressed into wafers.

Immediately preceding the recording of XAS spectra, samples were cooled rapidly to liquid nitrogen temperature. The spectra $\mu(k)$ were measured in transmission mode using ionization chambers. A metal foil (between the second and the third ionization chamber) was measured at the same time for energy calibration purposes. Data treatment was carried out using the software package VIPER.[27] For background subtraction, a Victoreen polynomial was fitted to the preedge region. A smooth atomic background $\mu_0(k)$, was evaluated using smoothed cubic splines. The radial distribution function FT-$[k^2\chi(k)]$ was obtained by Fourier transformation of the k^2-weighted experimental function $\chi(k) = (\mu(k) - \mu_0(k))/\mu_0(k)$ multiplied by a Bessel window. Duplicate spectra were recorded to ensure data reproducibility.

Nanocrystalline α-Ni$_{1−x}$Al$_x$ (0.09 ≤ x ≤ 0.50) and β-NiAl Powders from $[Ni(cod)_2]$ and $[(AlCp^*)_4]$. Samples of 0.200 g of $[Ni(cod)_2]$ (0.727 mmol) and the corresponding molar amount x of $[(AlCp^*)_4]$, calculated for the desired composition of α-Ni$_{1−x}$Al$_x$ (see Table 1), were suspended in mesitylene (20 mL), using a Fischer−Porter bottle as reaction vessel. The bright yellow suspension was degassed, set under 3 bar of H_2 pressure, and placed into a 150 °C hot oil bath. The color immediately turned to orange, then bright red. After 1 min, a dark red solution formed, which rapidly turned red-brown. Whereas Ni-rich α-phase particles (0.09 ≤ x ≤ 0.33) precipitated within minutes, for $x = 0.50$ (NP1), the particles precipitated completely only after 10 h. The suspension was stirred over 4 days, while hydrogen was quantitatively consumed. The particles were allowed to settle, and the colorless supernatant was carefully decanted in the glovebox. The residue was washed with 3 × 50 mL of n-pentane. Thereafter, the residual solvent and the hydrocarbon byproducts were removed in vacuo and the black residue was thoroughly dried (1 h at 10^{-3} mbar/ 100 °C).

General Procedure for the Oxidation of α-Ni$_{1−x}$Al$_x$ Nanoparticles. All α-Ni$_{1−x}$Al$_x$ nanoparticles, synthesized and isolated as powder sample in the glovebox as described above, were transferred into glass vials which were left open in the box over night (H_2O and O_2 ≤ 1 ppm) in order to initiate gentle surface oxidation. Subsequently, the vials were taken out of the glovebox and exposed to air for 24 h at room temperature for quantitative surface oxidation.

Nanocrystalline β-NiAl Powder (NP2) from $[Ni(cod)_2]$ and $[(Me_3N)AlH_3]$. A solution of 0.065 mg of $[(Me_3N)AlH_3]$ (0.727 mmol) in mesitylene (5 mL) was slowly added to a bright yellow mesitylene solution of 0.200 g of $[Ni(cod)_2]$ (0.727 mmol) in a Fischer−Porter bottle. The solution immediately turned to dark red, and after complete addition, a black powder precipitated, accompanied with gas production. The bottle was pressurized with 3 bar of H_2 and heated at 150 °C for 24 h. Thereafter, the bottle was transferred into the glovebox, where the powder was allowed to settle. Subsequently, the colorless solution was decanted, and the residue was washed with 3 × 20 mL of n-pentane and dried. Yield: 0.057 g (87%, based on Ni). Elemental analysis, wt %: Ni, 54.2; Al, 24.8; C, 16.6; H, 3.2; O, 1.2 (calculated from difference to 100 wt %).

Nanocrystalline β-NiAl Colloids (NP3) from $[Ni(cod)_2]$ and $[(AlCp^*)_4]$. In a Fischer−Porter bottle, 0.200 g of $[Ni(cod)_2]$ (0.727 mmol) and 0.118 g of $[(AlCp^*)_4]$ (0.182 mmol; 0.728 mmol for monomeric AlCp*) were combined in mesitylene (20 mL). The bright yellow suspension was degassed, set under 3 bar of H_2 pressure, and stirred at 150 °C. The color immediately turned to orange, then bright red. After 1 min, a dark red solution formed, which rapidly turned red-brown. The solution was stirred at

(24) Krysan, D. J.; Mackenzie, P. B. *Inorg. Chem.* **1990**, *55*, 4229−4230.

(25) Schormann, M.; Klimek, K. S.; Hatop, H.; Varkey, S. P.; Roesky, H. W.; Lehmann, C.; Röpken, C.; Herbst-Irmer, R.; Noltemeyer, M. *J. Solid State Chem.* **2001**, *126*, 225−236.

(26) Jouet, R. J.; Warren, A. D.; Rosenberg, D. M.; Bellitto, V. J.; Park, K.; Zachariah, M. R. *Chem. Mater.* **2005**, *17*, 2987−2996.

(27) Klementiev, K.V. *VIPER for Windows*, Visual Processing in EXAFS Researches, freeware, www.desy.de/~klmn/viper.html.
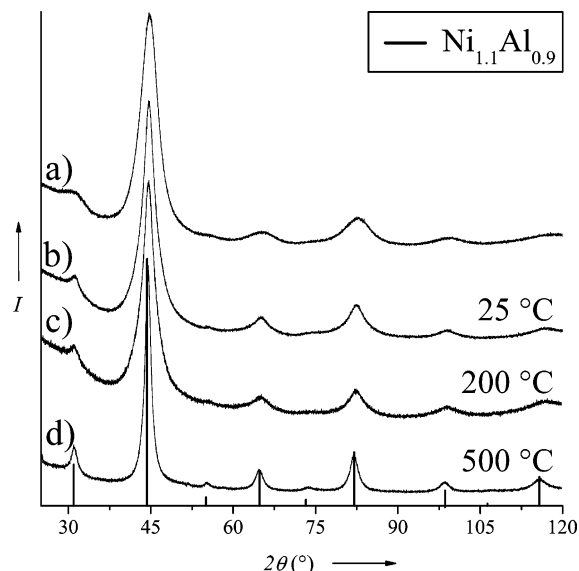
Figure 1. XRD diagrams of (a) β-Ni$_{1.1}$Al$_{0.9}$ NP2, synthesized from [Ni(cod)$_2$] and [(Me$_3$N)AlH$_3$], (b) β-Ni$_{1.1}$Al$_{0.9}$ NP1, synthesized from [Ni(cod)$_2$] and [(AlCp*)$_4$], (c) NP1 annealed at 200 °C, and (d) NP1 annealed at 500 °C.

150 °C for 8 h without the occurrence of precipitation. Prolonged stirring at 150 °C beyond 10 h of reaction time would lead to precipitation. The solvent and the hydrocarbon byproducts were removed in vacuo as described above. Yield: 0.072 g (116%). The solvent and the hydrocarbon byproducts were removed in vacuo. Yield: 0.072 g (116% based on Ni). Elemental analysis, wt %: Ni, 42.1; Al, 19.7; C, 32.0; H, 4.0; O, 2.2 (calculated from difference to 100 wt %).

ACA-Stabilized β-NiAl Colloids (NP4). NiAl colloids (0.072 g, 0.727 mmol) were synthesized in mesitylene (20 mL) as described above. After 8 h of hydrogenation (no precipitate), the Fischer–Porter bottle was transferred into the glovebox, where 0.065 g of ACA (0.363 mmol, 0.5 equiv) was added. The initially brown-black colored solution changed to dark red. The solution was stirred overnight at 150 °C in an argon atmosphere. The solvent was removed in vacuo, and the black, metallic shiny solid was dried as described above. Yield: 0.113 g (82% based on Ni). Elemental analysis, wt %: Ni, 29.8; Al, 14.1; C, 39.1; H, 4.6; O, 12.4 (calculated from difference to 100 wt %).

Results and Discussion

Nanocrystalline β-NiAl by Cohydrogenolysis of [Ni(cod)$_2$] with [(AlCp*)$_4$] or [(Me$_3$N)AlH$_3$]. *Synthesis.* The cohydrogenolysis of equimolar amounts of [Ni(cod)$_2$] (**1**) and [(AlCp*)$_4$] (**2**) under 3 bar of H$_2$ pressure in mesitylene at 150 °C without any other additives leads to the formation of a brown-black solution, which is stable for 8–10 h under the reaction conditions. After 10 h, the solution becomes colorless and a black powder precipitates. The suspension was stirred for 4 days, while a complete loss of H$_2$ pressure was observed. The colorless supernatant was decanted, and the powder was washed with *n*-pentane and thoroughly dried in high vacuo at 100 °C. The obtained extremely pyrophoric powder was characterized by means of XRD as apparently phase-pure β-Ni$_{1.1}$Al$_{0.9}$, in the following denoted as NP1 (cubic, *Pm3m*, JCPDS no. 44-1187, Figure 1b). The average crystallite domain size was roughly estimated to be 4 ± 1 nm via the Scherrer equation based on the full widths at half-maximum (fwhm) of the (111), (110), (200), and (211)

Scheme 1. Cohydrogenolysis of [Ni(cod)$_2$] and [(AlCp*)$_4$] or [(Me$_3$N)AlH$_3$] to β-NiAl Nanoparticles
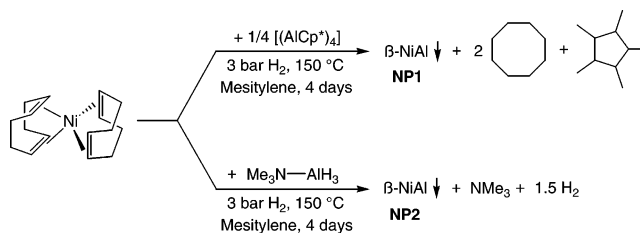
reflections. Reflections of elemental Ni or Al were not visible, even after annealing at 500 °C, pointing to a quantitative alloying. The organic byproducts of the cohydrogenolysis being dissolved in the mesitylene supernatant were characterized by GC–MS and NMR (^{1}H, ^{27}Al). The GC–MS analysis revealed cyclooctane (**4**), 1,2,3,4,5-pentamethylcyclopentane (**5**), and 1,3,5-trimethylcyclohexane (**6**) besides mesitylene. Thus, during the decomposition of the precursors, the ligands 1,5-cyclooctadiene and 1,2,3,4,5-pentamethylcyclopentadiene and, to some extent, the solvent itself were hydrogenated. In the ^{1}H NMR spectrum, the signal of **4** appears at 1.51 ppm, which is in good accordance to literature reports. The signals of **5** and **6** appear as a variety of multiplets in the range between 1.2 and 0.3 ppm, since the methyl groups of **6** can adopt both axial and equatorial positions. Most importantly, the ^{27}Al NMR of the supernatant does not exhibit any signals so that it can be concluded that there were no significant amounts of remaining [(AlCp*)$_4$] and other soluble Al-containing side products. Summing up, we propose Scheme 1 for the synthesis of β-NiAl from **1** and **2**.

Alternatively, the synthesis of β-NiAl can also be performed with [(Me$_3$N)AlH$_3$] (**3**) as a more readily accessible Al source.[26,28] Compound **3** is a well-known precursor for Al in thin film technology, i.e., chemical vapor deposition of thin Al films.[29] It has also been used for the preparation of Al nanoparticles before.[26,28] Treating a solution of [Ni(cod)$_2$] (**1**) in mesitylene with an equimolar amount of **3** at 25 °C leads to an immediate reaction, upon which a black powder precipitates instantaneously. The suspension was then set at 3 bar of H$_2$ and heated to 150 °C for 1 day. The particles were isolated by means of filtration and were washed with *n*-pentane and dried as described before. The organic products of the cohydrogenolysis, cyclooctane (from the hydrogenation of the cod ligand) and NMe$_3$ (from the decomposition of the Al precursor), were found in the filtrate. The XRD diagram of the obtained air-sensitive powder again confirms the presence of the β-NiAl phase (NP2, Figure 1a). The crystallite size is very small, having a diameter of around 3 nm, as calculated from the fwhm of the (110) reflection.

The combination of labile all-hydrocarbon metal precursors ML$_n$ such as [Ni(cod)$_2$] (with cod = L; *n* = 2) with [(Me$_3$N)AlH$_3$] (**3**) is quite similar to the established route of treating metal halides MX$_n$ with LiAlH$_4$ cited in the Introduction.

(28) (a) Haber, J. A.; Buhro, W. E. *J. Am. Chem. Soc.* **1998**, *120*, 10847–10855. (b) Higa, K. T.; Johnson, C. E.; Hollins, R. A. U.S. Patent 5,885,321, 1999.

(29) (a) Gladfelter, W. L.; Boyd, D. C.; Jensen, K. F. *Chem. Mater.* **1989**, *1*, 339–343. (b) Weiss, J.; Himmel, H.-J.; Fischer, R. A.; Wöll, C. *Chem. Vap. Deposition* **1998**, *4*, 17–21.

Similarly, Bogdanović et al. used catalytically prepared solid or solubilized magnesium hydride (MgH_2) to prepare amorphous binary magnesium intermetallics.[30] This avoids the formation of LiCl as an only partly soluble (in organic solvents) solid-state byproduct. However, the reactions with suitable all-hydrocarbon transition metal precursors with the main group hydrides may be very vigorous. For example, $[Ni(cod)_2]$ reacts with $[(Me_3N)AlH_3]$ even in the solid state upon mixing without any solvent! The advantage of the less common Al precursor $[(AlCp*)_4]$ (**2**) over $[(Me_3N)AlH_3]$ (**3**) is the option of tuning and better adjustment of the reaction kinetics of nucleation and particle growth.

Characterization. According to elemental analysis of one representative sample, the NP1 particles contain 50.9 wt % Ni and 23.1 wt % Al, which corresponds to a Ni/Al stoichiometry of 1.013:1.000, or the sum formula $Ni_{0.503}Al_{0.497}$. The significant C and H contents of 23.4 wt % and 2.6 wt %, respectively (C/H molar ratio of 1.00:1.32), suggest the presence of mesitylene (C_9H_{12}, C/H ratio 1.00:1.33). The IR spectrum of a sample of NP1 exhibits only quite weak absorptions (see the Supporting Information). This observation is in qualitative agreement with the mesitylene traces in the powder. The preparation of β-NiAl from **1** and **2** was repeated several times, and the measured β-NiAl reflections exhibited slight shifts corresponding to a variation in compositions of $Ni_{0.55}Al_{0.45}$, $Ni_{0.52}Al_{0.48}$, $Ni_{0.50}Al_{0.50}$, and $Ni_{0.45}Al_{0.55}$. The random deviations of the lattice constants in comparison to the literature reference $Ni_{0.50}Al_{0.50}$ is pointing to slight variations of the molar Ni/Al ratio in the synthesis. The very accurate determination of the molar ratio of the particular organometallic precursors by weighing and the quantitative transfer into the reaction vessel is more difficult than is usually the case when highly pure elemental metals or simple inorganic compounds are the starting materials. Nevertheless the inaccuracy of the obtained compositions of less than ±5% appears quite good. A representative sample of NP1 was annealed in a sealed quartz tube in vacuo for 24 h at 200 °C and also at 500 °C, respectively. No other reflections than those of the β-NiAl phase were detected (Figure 1c). In the case of the sample annealed at 200 °C, the average particle size of 4 nm does not differ from the as-synthesized particles. Upon annealing at 500 °C some sintering took place leading to a typical size of the crystallites of 8 nm (Figure 1d). Presumably, during the synthesis and the workup of the NiAl material, a thin Al_2O_3 layer, formed from traces of oxygen or water (e.g., in the solvent), inhibits particle growth (see the elemental analysis data and the respective section below).

The TEM image of the particles NP1 reveals broad sections of agglomerates, consisting of small primary particles, which confirm the crystallite size calculation from XRD data (Figure 2, left image), which is pointing to polycrystalline particles. In an HRTEM image, a faint shell around the particle is visible (Figure 2, right); however, it was not possible to determine whether it is an alumina shell,
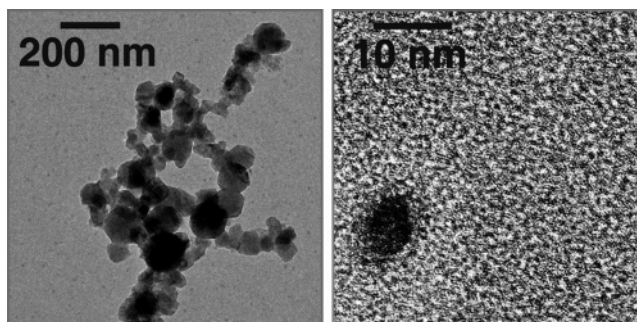

Figure 2. TEM images of agglomerates of nano-β-NiAl NP1 (left) and a zoom on a single NP1 particle (right).

formed upon sample preparation by air oxidation, or (hydro)-carbon residues from the synthesis. The results of the EDX (energy-dispersive X-ray) analysis of verify the Ni/Al ratio of around 1:1, within the accuracy of the method of measurement of ±10%. The analyses of several particle regions did not show significant deviations from the Ni/Al ratio of 1:1. It should be noted, that Ni- or Al-rich particles, as well as Ni- or Al-only regions, could not be found.

Nonaqueous Colloids of β-NiAl Nanoparticles (NP3). *Synthesis.* As mentioned above, the cohydrogenolysis of $[Ni(cod)_2]$ (**1**) and $[(AlCp*)_4]$ (**2**) leads to a brown-black solution, which is stable up to 8 h of reaction time, and beyond 8−10 h, β-NiAl particles are precipitating. Noteworthy, after 8 h, the entire hydrogen pressure is consumed as indicated by a drop of the pressure from 3 to ≤0.1 bar. The reaction was followed by NMR, but the reaction mixture was strongly paramagnetic so that no NMR spectrum could be recorded. This observation is a hint on the formation of Ni particles or clusters, since the Ni precursor decomposes at a faster rate than AlCp*. In the context of our work on the coordination chemistry of low-valent group 13 organyls ECp* (E = Al, Ga, In) on d^{10} metal centers,[31] we found that in an inert gas atmosphere, $[Ni(cod)_2]$ quantitatively reacts with an excess of $[(AlCp*)_4]$ to the thermodynamically stable complex $[Ni(AlCp*)_4]$, which, however, is not paramagnetic.[32] Besides, the reaction of equimolar amounts of $[Ni(cod)_2]$ and GaCp* under dihydrogen yields the distorted cubic Ni_8 cluster $[Ni_8(GaCp*)_6]$.[33] As the two precursors **1** and **2** decompose at different time scales, it is reasonable to assume the formation of AlCp*-stabilized Ni clusters at an early stage of the reaction, besides the parallel decomposition of $[Ni(cod)_2]$, before splitting off the Cp*H from the Al centers and formation of the alloy.

In order to characterize the described intermediate black-brown solution, the mixture was cooled down from 150 °C to room temperature after 8 h and the all volatile components were removed in high vacuo, whereupon a black, metallic shining residue (NP3) remained. These particles can easily be redispersed in aromatic solvents, such as benzene, toluene, or mesitylene. The liquid phase was studied by ^1H NMR. Besides signals of the remaining solvent at 6.67 and 2.13

(30) (a) Bogdanović, B.; Liao, S.; Schwickardi, M.; Sikorsky, P.; Spliethoff, B. *Angew. Chem., Int. Ed. Engl.* **1980**, *19*, 818−819. (b) Bogdanović, B.; Claus, K.-H.; Gürtzgen, S.; Spliethoff, B.; Wilczok, U. *J. Less-Common Met.* **1987**, *131*, 163−172.

(31) (a) Gemel, C.; Steinke, T.; Cokoja, M.; Kempter, A.; Fischer, R. A. *Eur. J. Inorg. Chem.* **2004**, 4161−4176. (b) Steinke, T.; Gemel, C.; Winter, M.; Fischer, R. A. *Chem. Eur. J.* **2005**, *11*, 1636−1646.

(32) Steinke, T.; Gemel, C.; Cokoja, M.; Winter, M.; Fischer, R. A. *Angew. Chem., Int. Ed.* **2004**, *43*, 2299−2302.

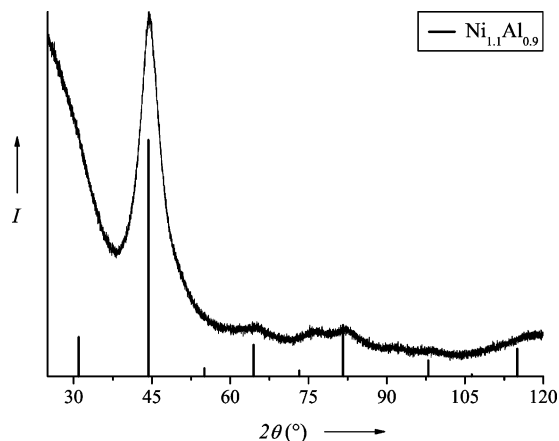(33) Steinke, T.; Gemel, C.; Fischer, R. A. Unpublished results.

Figure 3. XRD diagram of β-NiAl nanoparticles (NP3), isolated from a colloidal solution.
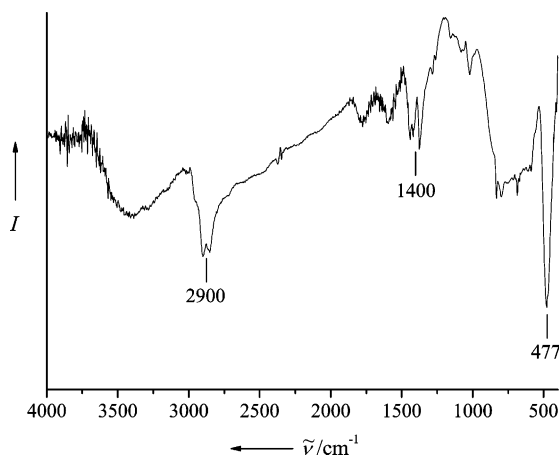

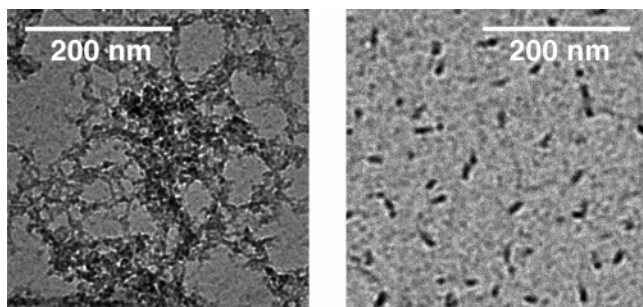**Figure 4.** IR spectrum of NiAl nanoparticles NP3.

Figure 5. TEM images of NiAl colloids without surfactant (NP3, left) and with 1-adamantane carboxylic acid as surfactant (NP4, right).

ppm, a very broad resonance between 2.5 and 1.0 ppm is visible. The ^{13}C NMR spectrum reveals only one weak resonance at 21.3 ppm, pointing to aliphatic CH_2 or CH_3 groups. The ^{27}Al NMR spectrum exhibits no signals so that undesired side reactions of AlCp*, e.g., oxidation of Al(I), can be ruled out.

Characterization. XRD analysis confirms that the obtained powder consists of β-NiAl nanoparticles (Figure 3). The reflections are very broad as compared with the samples of Figure 1 and thus imply a crystallite domain size below 4 nm. On the basis of the fwhm of the (110) reflection only, the average size of crystalline domains was roughly estimated to about 2 nm.

The NiAl colloids NP3 were studied by TEM (Figure 5, left image, vide infra), showing a rather poor dispersion of

a network of small particles, in spite of the observed quite good solubility and redispersability of the isolated NP3 material. The unexpected stability of the as-synthesized NiAl nanoparticles as a colloidal solution without the presence of any intentionally added surfactant is surprising. The subsequently precipitated, washed, and dried NiAl powder material analyzed to 42.1 wt % Ni and 19.7% Al (Ni/Al ratio of 1.000: 1.018) around 36 wt % of hydrocarbons (32.0% C, 4.2% H, C/H ratio 1.00:1.56). The obtained mass yield of NP3 is 117% of the expected mass of the pure metals after quantitative decomposition. NMR and IR measurements of a sample of NP3 were undertaken. In contrast to NP1, the IR spectrum, shown in Figure 4, reveals broad aliphatic C–H vibration bands at around 2900 and 1300–1500 cm^{-1} and a very strong Al–C vibration band arising at 477 cm^{-1}.

Thus, it can be concluded that the particles are accompanied by an undefined, presumably high molecular mass organic product, which has a weak interaction with the particle surface but allows the dispersion of the particles in organic solvents, such as *n*-hexane or toluene. Few groups have reported on the phenomenon of the stability of colloidal metal nanoparticles in presence of nonfunctionalized surfactants, having no distinct covalent or ionic/electrostatic interaction with the particle surface. Recently, we have shown that the thermal codecomposition of [Cu(OCH(Me)CH$_2$-NMe$_2$)$_2$] and [ZnEt$_2$] in 200 °C hot squalane (2,6,10,15,19,-23-hexamethyltetracosane) yields free-standing ZnO@Cu colloids, which, however, gradually precipitate after prolonged storage under argon.[34] Tristany et al. synthesized Ru nanoparticles stabilized by perfluorohexacosane.[35] In the case of our NiAl colloids, the surfactant is presumably a product of ring opening of the Cp* ligand and subsequent oligomerization, catalyzed by Ni or NiAl. This hypothesis is, for example, substantiated by the work of Rabinovich et al. who observed the ring opening of cyclopentadiene over a Pt/Al$_2$O$_3$ catalyst at 500 °C to 1,3-pentadiene, which can further form longer chains.[36] Besides, di-, tri-, and tetramerization Diels–Alder products were also observed. Coordination of some not yet decomposed AlCp* to the surface of the NiAl particles may also be taken into account.

Olefin Hydrogenation Catalyzed by β-NiAl Nanoparticles (NP3). The loss of the *excess* hydrogen pressure occurs *after* the quantitative formation of NiAl nanoparticles. Thus, it seems that the supposedly initially formed Ni particles are not solely responsible for the hydrogenation, but rather the formed NiAl nanoparticles are also quite active hydrogenation catalysts as well. Petró et al. reported on the catalytic activity of NiAl powder for hydrogenation on the examples of various organic compounds, e.g., nitrobenzene, acetophenone, eugenol, and benzonitrile.[37] Hence, the catalytic activity of the β-NiAl nanoparticles (NP3) for cyclohexane hydrogenation as a test case was studied. Thus, a sample of NP3

(34) Schröter, M. K.; Khodeir, L.; van den Berg, M. W. E.; Hikov, T.; Cokoja, M.; Miao, S.; Grünert, W.; Muhler, M.; Fischer, R. A. *Chem. Commun.* **2006**, 2498–2500.
(35) Tristany, M.; Chaudret, B.; Dieudonné, P.; Guari, Y.; Lecante, P.; Matsura, V.; Moreno-Mañas, M.; Philippot, K.; Pleixats, R. *Adv. Funct. Mater.* **2006**, *16*, 2008–2015.
(36) Rabinovich, G. B.; Bakulin, R. A.; Glinchak, S. I. *Neftekhimiya* **1989**, *29*, 751–755.
(37) Petró, J.; Hegedüs, L.; Sajó, I. E. *Appl. Catal., A* **2006**, *308*, 50–55.

(0.35 mmol) was suspended in 5 mL of cyclohexene (50 mmol) and treated with 3 bar of H_2 at 100 °C, whereupon a rapid pressure loss was observed. Hydrogen was added as long as the pressure would not decrease any longer. The total consumption of 14.6 bar of H_2 nicely corresponds to 50 mmol of cyclohexene, which points to a complete hydrogenation to cyclohexane. The solvent was distilled off, and an aliquot was taken for a ^1H NMR measurement. The spectrum (see the Supporting Information) exhibits only one singlet at 1.40 ppm, which is in agreement with literature data for cyclohexane. Signals of cyclohexene were not observed, indicating the completed hydrogenation.

Nonaqueous Colloids of 1-Adamantanecarboxylic Acid Stabilized α-NiAl Nanoparticles. *Synthesis.* Isolated β-NiAl nanoparticles NP3 can be redispersed in toluene and can be stored in a Schlenk vessel under argon for several days without any precipitation. However, the particles tend to agglomerate and are polydisperse (TEM, see Figure 5). Apparently, the organic shell is too weakly bound to keep the particles in solution for a longer period of time. Previous experiments of the cohydrogenolysis of [CpCu(PMe₃)] and [(AlCp*)₄] in the presence of common surfactants like hexadecylamine (HDA) or trioctylphosphineoxide (TOPO) did not give stable colloids.[21] It is noteworthy that after all efforts, it was not possible to stabilize Al nanoparticles as colloids, by use of various surfactants. The hydrogenolysis of [(AlCp*)₄] in presence of HDA, which is one of the most frequently used stabilizing capping ligands, resulted in the formation of a solution of a Al(III) species, according to ^{27}Al NMR measurements.[21] The use of PVP as colloid matrix resulted in the formation of Al_2O_3, presumably due to the reaction of AlCp* with the ring carbonyl group. Sterically demanding carboxylic acids, such as 1-adamantanecarboxylic acid (ACA), or fatty acids, such as oleic acid (OLEA) or stearic acid, represent well-known examples of efficient, yet chemically inert surfactants, which allow a control over the particle shape and assembly. However, in all cases, they stabilize oxidation-stable metal and alloy colloids such as CoPt₃,[38] FePt,[39] and NiPt,[40] but as well metal oxides, e.g., TiO₂,[41] when applied as an additive *during* synthesis. The presence of quantitative amounts of Brønsted acids, as well as primary amines (vide supra) or alcohols, immediately leads to side reactions with the Al precursors **2** or **3** to form stable Al(III) species, which cannot be decomposed to Al(0), at least not under the conditions described. Lower amounts of ACA (e.g., 0.1 equiv), however, cannot prevent the precipitation of Al nanoparticles or Al alloys. Hence, we decided
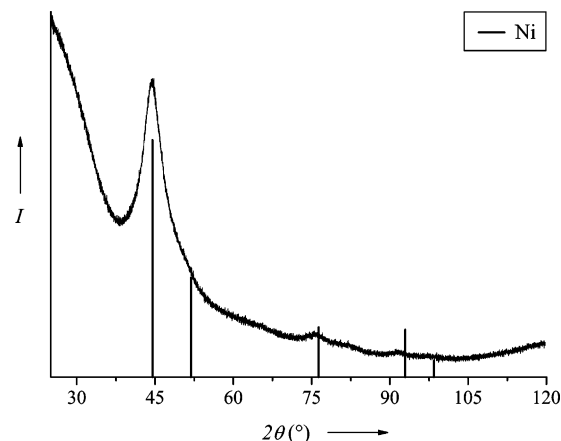

Figure 6. XRD diagram of ACA-stabilized Ni/Al colloids NP4.

to use ACA as a postsynthesis additive to bind on the particle surface for a better dispersion of the colloids. Assuming a spherical shape of a colloidal β-NiAl particle of the type NP3 with a diameter of around 2 nm (estimated by XRD), 60 molecules of ACA (diameter ~5 Å) should be sufficient to entirely cover its surface, which roughly corresponds to a NiAl/ACA molar ratio of 2:1. On the basis of that estimation, the brown-black solution of stoichiometric β-NiAl nanoparticles in mesitylene ($c = 36$ mmol/L) was treated with 0.5 equiv of ^{17}O-enriched ACA, whereupon the color changed to deep red. The solution was stirred for 16 h at 150 °C without further color change or precipitation. Upon evaporation of the solvent in vacuo at 100 °C, a black, shiny powder was isolated. The powder was easily redispersed in aromatic solvents and proved to be stable under argon for several weeks in contrast to the original NP3 sample. The admittance of trace amounts of oxygen, however, led to a rapid precipitation.

Characterization. According to elemental analysis, the ACA@Ni/Al sample, denoted as NP4, contains 29.8 wt % Ni and 14.1 wt % Al, as well as 39.1 wt % C and 4.6 wt % H. The residual weight percentage of 12.4 can be assigned to oxygen. This result corresponds to an empirical formula for NP4 as $Ni_{1.00}Al_{1.03}C_{6.41}H_{8.99}O_{1.51}$. Taking into account that the sample may still contain traces of mesitylene (C_9H_{12}) and that rigorous exclusion of unintentional oxidation cannot be guaranteed, this formula is in acceptable agreement to a molar ratio of NiAl/ACA of 2:1 (corresponding to $Ni_{1.00}Al_{1.00}C_{5.50}H_{8.00}O_{1.00}$; ACA: $C_{11}H_{16}O_2$).

The XRD pattern of the particles NP4 reveals very broad reflections that can be assigned to the fcc-Ni structure (Figure 6). Yet, the reflections exhibit small shifts in comparison to the fcc-Ni reference data, indicating the presence of another component in the Ni lattice. According to the binary Ni–Al phase diagram and quite typical for Hume–Rothery phases, the β-NiAl phase is stable in a range of 40–55 atom % Al at ambient conditions, and the α-Ni phase region dominates below 40%.[42] The deviation of the lattice constant from the Ni reference allows an estimation of the molar fraction of Al(0) dissolved in the lattice of Ni which turns out to be around 38 ± 4 atom % in our case. (Vegard's law, vide

(38) (a) Shevchenko, E. V.; Talapin, D. V.; Murray, C. B.; O'Brien, S. *J. Am. Chem. Soc.* **2006**, *128*, 3620−3637. (b) Shevchenko, E. V.; Talapin, D. V.; Schnablegger, H.; Kornowski, A.; Festin, Ö.; Svedlinh, P.; Haase, M.; Weller, H. *J. Am. Chem. Soc.* **2003**, *125*, 9090−9101. (c) Shevchenko, E. V.; Talapin, D. V.; Rogach, A. L.; Kornowski, A.; Haase, M.; Weller, H. *J. Am. Chem. Soc.* **2002**, *124*, 11480−11485.
(39) (a) Kang, S.; Jia, Z.; Shi, S.; Nikles, D. E.; Harrell, J. W. *Appl. Phys. Lett.* **2005**, *86*, 026503-1−026503-3. (b) Sun, S.; Murray, C. B.; Weller, D.; Folks, L.; Moser, A. *Science* **2000**, *287*, 1989−1992. (c) Sra, A. K.; Ewers, T. D.; Xu, Q.; Zandbergen, H.; Schaak, R. E. *Chem. Commun.* **2006**, 750−752.
(40) Ahrenstorf, K.; Albrecht, O.; Heller, H.; Kornowski, A.; Görlitz, D.; Weller, H. *Small* **2007**, *3*, 271−274.
(41) Cozzoli, P. D.; Kornowski, A.; Weller, H. *J. Am. Chem. Soc.* **2003**, *125*, 14539−14548.

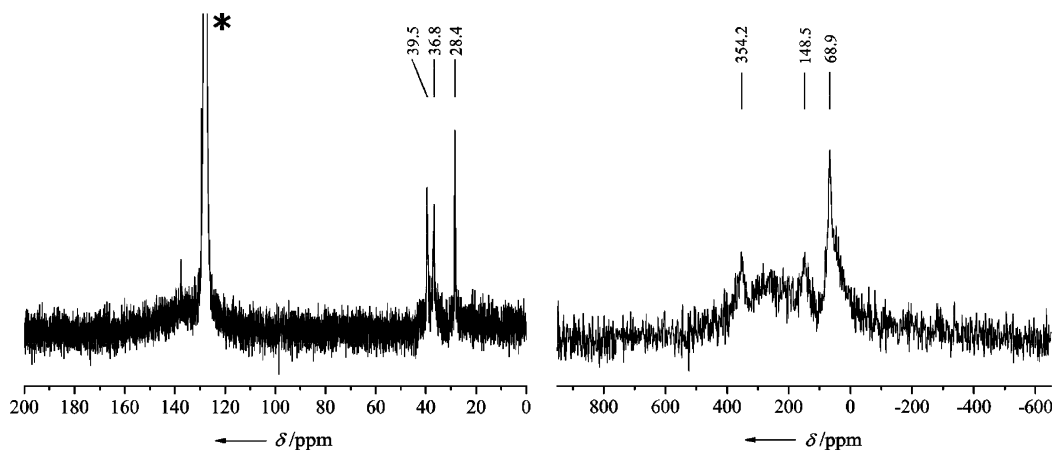(42) Hansen, M., Ed. *Constitution of Binary Alloys*, 2nd ed.; McGraw-Hill: New York, 1958.

Figure 7. ^{13}C NMR spectrum (left) and ^{17}O NMR spectrum (right) of ACA@Ni/Al colloids (NP4) in C_6D_6 solution. The asterisk in the left spectrum marks the ^{13}C signal of C_6D_6 at 128 ppm.
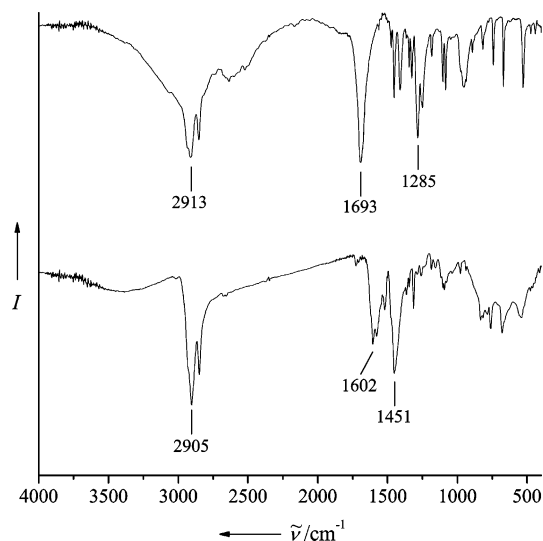

Figure 8. IR spectrum of free ACA (top) and ACA coordinated at the surface of NiAl particles NP4 (bottom).

infra).[43-46] From this observation we conclude that some of the Al has been enriched at the surface in the course of the ACA addition. The average crystallite size is approximately 2 nm, calculated from the fwhm of the (111) reflection. The other reflections were too weak and broad to be used for reliable size estimation via the Scherrer equation.

The ^{1}H NMR spectrum of NP4 in C_6D_6 displays numerous broad signals between 2.5 and 1.0 ppm, and it is difficult to unambiguously locate the protons of the ACA surfactant. The absence of the carboxyl proton indicates the conversion of the acid to a carboxylate. The absence of the IR carbonyl vibration band of the free acid (Figure 8, top) at 1693 cm^{-1} confirms the formation of carboxylate species adsorbed at the particle surface (Figure 8, bottom). As already deduced from the elemental analysis data, the NMR spectrum exhibits the expected traces of mesitylene. In the ^{27}Al NMR spectrum, no signals could be detected. In the ^{13}C NMR spectrum (Figure 7, left) only the resonance shifts of the adamantyl carbons at 39.5, 36.8, and 28.4 ppm were visible. The signals

of the carboxylate carbon and the neighbored C atom were not detected. This is not surprising, since it is well documented that, for colloidal ligand-stabilized nanoparticles, the α- and β-carbons and -protons of the ligand cannot be detected by NMR.[47] Since the nanoparticle behaves as a solid material, the atoms bound to the surface exhibit a chemical shift anisotropy of the dipole−dipole interactions, resulting from the slow tumbling of the particles in solution (in contrast to discrete molecules), which are not averaged as in the case of molecules in solution. This causes a very strong line broadening. The ^{17}O NMR spectrum (Figure 7, right) shows two weak signals at 354.2 and 148.5 ppm. In addition, a very broad structure is extending between 500 and −100 ppm and a strong resonance at 68.9 ppm that stems from Al_2O_3, according to literature reports on the ^{17}O MAS NMR shift of alumina.[44] The signal of the free acid at 247.5 ppm (authentic reference sample in C_6D_6) is not visible, concluding that the ACA is quantitatively attached to the particle surface.

The signal splitting of the adamantane carboxylate in two peaks at 354.2 and 148.5 ppm indicates nonequivalent oxygen atoms and thus possibly suggests a unidentate coordination mode at the particle surface. Tao studied the coordination behavior of monolayers of carboxylic acids on Cu, Ag, and Al surfaces.[45] All examined films form oxide layers when exposed to air, and the basicity of the metal oxide seems to have an influence of the binding mode of the acid, whereas the carboxylate ligand is binding in bidentate fashion at Cu and Ag, it is binding with one oxygen on an Al surface, as shown by reflection absorption IR spectrometry (RAIRS) measurements. Deacon and Phillips examined the carboxyl IR vibration bands of numerous transition metal carboxylate complexes and showed that an asymmetric R−COO coordination, i.e., unidentate, gives rise to an increase of the difference of the

(43) Dale, H.; Vegard, L. *Z. Kristallogr., Kristallgeom., Kristallphys., Kristallchem.* **1928**, *67*, 148−161.
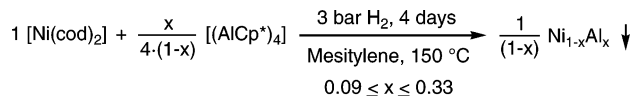(44) Bastow, T. J.; Stuart, S. N. *Chem. Phys.* **1990**, *143*, 459−467.
(45) Tao, Y.-T. *J. Am. Chem. Soc.* **1993**, *115*, 4350−4358.
(46) Deacon, G. B.; Phillips, R. J. *Coord. Chem. Rev.* **1980**, *33*, 227−250.

(47) (a) Chaudret, B. Private communication. (b) Dassenoy, F.; Phillipot, K.; Ould Ely, T.; Amiens, C.; Lecante, P.; Snoeck, E.; Mosset, A.; Casanove, M.-J.; Chaudret, B. *New J. Chem.* **1998**, 703−711. (c) Pelzer, K. Ph.D. Thesis, Universität-GH Essen, 2003. (d) Badia, A.; Gao, W.; Singh, S.; Cuccia, L.; Reven, L. *Langmuir* **1996**, *12*, 1262−1269. (e) Terrill, R. H.; Postlethwaite, T. A.; Chen, C.; Poon, C.-D.; Terzis, A.; Chen, A.; Hutchinson, J. E.; Clark, M. R.; Wignall, G.; Londono, J. D.; Superfine, R.; Falvo, M.; Johnson, C. S.; Samulski, E. T.; Murray, R. W. *J. Am. Chem. Soc.* **1995**, *117*, 12537−12548.

Scheme 2. Wet Chemical Synthesis of α-Ni$_{1-x}$Al$_x$ Nanoparticles

$$1 \text{ [Ni(cod)}_2] + \frac{x}{4 \cdot (1-x)} \text{[(AlCp*)}_4] \xrightarrow[\text{Mesitylene, 150 °C}]{\text{3 bar H}_2\text{, 4 days}} \frac{1}{(1-x)} \text{Ni}_{1-x}\text{Al}_x \downarrow$$
$$0.09 \leq x \leq 0.33$$

wavenumbers of the symmetric ($\tilde{\nu}_s$) and the asymmetric ($\tilde{\nu}_a$) COO stretching band, whereas a rather low $\tilde{\nu}_a$(COO)−$\tilde{\nu}_s$(COO) difference (<100 cm^{-1}) indicates a symmetric bidentate coordination.[46]

In Tao's work, the two vibration bands of COO coordinating at Al exhibit a wavenumber difference of 133 cm^{-1}. In the case of the ACA-stabilized Ni/Al particles NP4, $\tilde{\nu}_a$(COO)−$\tilde{\nu}_s$(COO) is 151 cm^{-1} (Figure 8, bottom). Jouet et al. reported on the coordination of long-chained perfluorocarboxylic acids on the surface of Al nanoparticles.[26] The $\tilde{\nu}_a$(COO)−$\tilde{\nu}_s$(COO) difference was found to be 185 cm^{-1}, with R−COO bridging two different Al atoms. Hence, a unidentate or bridging coordination of ACA would explain the carboxylate signal splitting in the ^{17}O NMR. However, capping ligands such as carboxylic acids are strongly bound to a particle surface, particularly on Al, being very rigid and thus should exhibit very weak signals in standard solution NMR.[47] In principle, these ligands can be detected by MAS NMR; however, in our case, ^{17}O MAS NMR did not reveal any signal apart from that of Al$_2$O$_3$, most presumably due to the low concentration and the low abundance of ^{17}O in the examined material. Thus, the actual signal of the ACA ligands on the particle surface may well be the broad signal, which extends over nearly 600 ppm. Summing up, the presented ^{17}O NMR data are not fully conclusive yet, and additional work is needed to clarify the binding mode of ACA to the particle surface. Nevertheless, the ^{13}C NMR and IR data support the assumption of ACA surface capping at the NiAl particles.

Nanocrystalline α-Ni$_{1-x}$Al$_x$ Powder Materials. The cohydrogenolysis of various molar ratios of [Ni(cod)$_2$] and [(AlCp*)$_4$] to α-Ni$_{1-x}$Al$_x$ phases ($0.09 \leq x \leq 0.50$) allows a free variation of the Al content in the aluminide alloy. Thus, the synthesis of Ni particles doped with Al was performed in analogy to the formation of β-NiAl nanopowder NP1 (Scheme 2).

In sharp contrast to the synthesis of β-Ni$_{0.50}$Al$_{0.50}$, the α-Ni$_{1-x}$Al$_x$ particles with $x \leq 0.33$ precipitate within minutes of H$_2$ pressure treatment. The initially bright yellow solution gradually changes the color over orange to bright red and finally dark red, before a black powder precipitates. The particles were isolated by filtration, washed with n-pentane, and dried. The actual atomic percentage of Al in the synthesized α-Ni$_{1-x}$Al$_x$ compounds slightly deviates from the Al content which was calculated from the mass of used [(AlCp*)$_4$], being 34.1% for the sample denoted with $x =$ 0.33 and 25.3% ($x = 0.25$), 17.0 ($x = 0.17$), and 8.2% ($x =$ 0.09) for the other samples, as shown by elemental analysis. The XRD diagrams of the α-Ni$_{1-x}$Al$_x$ samples ($0.09 \leq x \leq$ 0.33), presented in Figure 9, all exhibit very broad reflections that were assigned to the fcc-Ni structure (JCPDS no. 4-0850).

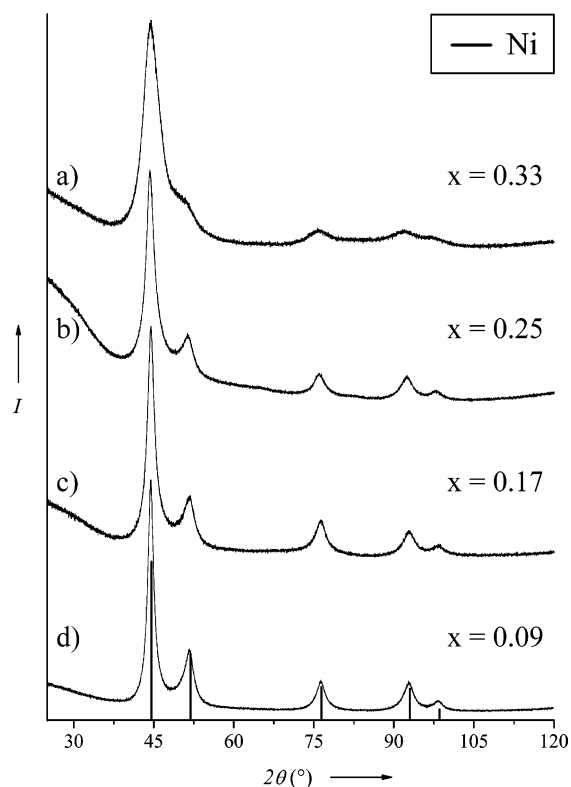The crystallite sizes of all measured α-Ni$_{1-x}$Al$_x$ samples do not show large deviations from those of the β-NiAl

Figure 9. XRD diagrams of (a) Ni$_{0.67}$Al$_{0.33}$, (b) Ni$_{0.75}$Al$_{0.25}$, (c) Ni$_{0.83}$-Al$_{0.17}$, and (d) Ni$_{0.91}$Al$_{0.09}$ α-phase nanoparticles, measured under argon.
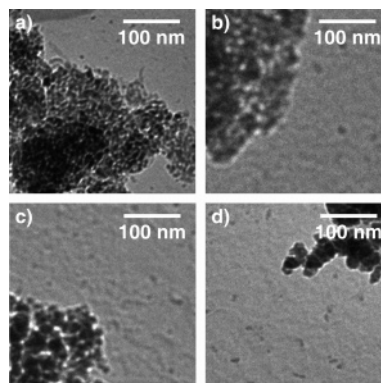

Figure 10. TEM images of (a) Ni$_{0.67}$Al$_{0.33}$, (b) Ni$_{0.75}$Al$_{0.25}$, (c) Ni$_{0.83}$Al$_{0.17}$, and (d) Ni$_{0.91}$Al$_{0.09}$ α-phase nanoparticles.

samples NP1 and NP2. From the fwhm of all observed reflections (apart from the (200) reflections), the average sizes of the crystallites in the measured α-Ni$_{1-x}$Al$_x$ powder samples were calculated to be 3 ± 1 nm for Ni$_{0.67}$Al$_{0.33}$, 7 ± 1 nm for Ni$_{0.75}$Al$_{0.25}$, and 8 ± 1 nm for Ni$_{0.83}$Al$_{0.17}$ and Ni$_{0.91}$-Al$_{0.09}$, respectively. This is consistent with the average size of primary particles which were observed by TEM (Figure 10, see below). With rising atomic percentage of Al, the XRD reflections exhibit an increasing shift from the fcc-Ni reference (Table 2), as a result of the growing distortion of the Ni lattice, which is caused by the incorporation of Al atoms. Noteworthy, it was not possible to obtain the γ'-Ni$_3$-Al phase by decomposition of 3 equiv of [Ni(cod)$_2$] with 1 equiv of [(AlCp*)$_4$]. The α-phase was formed, instead, indicating that the Al atoms are randomly distributed in the Ni lattice and thus do not form a well-ordered intermetallic phase of its own. Several groups reported on the synthesis

Table 1. Masses of [(AlCp*)$_4$] Required for the Desired Ni$_{1-x}$Al$_x$ Phases and the Yields

Ni$_{1-x}$Al$_x$	$m([(AlCp*)_4])$	elemental anal [wt %]	yield
$x = 0.50$	0.118 g (0.182 mmol)	Ni, 50.9; Al, 23.1	58 mg (93%)
$x = 0.33$	0.059 g (0.091 mmol)	Ni, 69.3; Al, 16.5	48 mg (91%)
$x = 0.25$	0.039 g (0.060 mmol)	Ni, 78.9; Al, 12.3	47 mg (96%)
$x = 0.17$	0.024 g (0.037 mmol)	Ni, 75.6; Al, 7.1	41 mg (86%)
$x = 0.09$	0.012 g (0.018 mmol)	Ni, 84.7; Al, 3.5	38 mg (84%)

of bulk Ni$_3$Al; however, in all cases, the samples were annealed at temperatures above 500 °C to obtain the desired γ'-Ni$_3$Al phase with the L1$_2$ structure.[48]

TEM measurements of the α-Ni$_{1-x}$Al$_x$ nanopowders (0.09 $\leq x \leq$ 0.33) shown in Figure 10 exhibit agglomerations of very small primary particles. The size of the primary particles appears to match to the size of crystallite domains, calculated from XRD, so that the synthesized samples can be regarded as nanocrystalline powders. The Ni/Al ratio, measured by EDX, was determined to be 2.6:1 for Ni$_{0.67}$Al$_{0.33}$, 3.5:1 for Ni$_{0.75}$Al$_{0.25}$, 4.5:1 for Ni$_{0.83}$Al$_{0.17}$, and 9.3:1 for Ni$_{0.91}$Al$_{0.09}$, within the accuracy of the method and matching the expectations.

The lattice constants of the α-Ni$_{1-x}$Al$_x$ nanoparticles were calculated via the Bragg equation from the (220) reflection, since the strongest (111) reflection did not show significant difference from the Ni reference in any case (Table 2). The second strongest reflection (200) overlapped with (111) for $x = 0.33$ so that the determination of the exact position of these reflections was not possible. The variation of the d-spacing (Table 1) with rising Al content follows Vegard's law (see the Supporting Information).

The evidently different agglomeration behavior of α-Ni$_{1-x}$Al$_x$ particles is in congruence with the decrease of concentration of AlCp* or Cp*, again suggesting that the Cp* moiety has a pronounced influence on the stabilization of the primary particles formed during cohydrogenolysis. It should be noted here, however, that precipitation of α-Ni$_{1-x}$Al$_x$ particles can in fact be prevented when polybutadiene ($M_w = 5000$ g/mol) is added during cohydrogenolysis of **1** and **2**. The characterization of the obtained α-NiAl colloids and the postsynthesis derivatization with ACA and other surfactants is underway and will be reported elsewhere.

Oxidation Behavior of α-Ni$_{1-x}$Al$_x$ Particles. *Oxidation.* In our previous work on colloidal α-Cu$_{1-x}$Al$_x$ nanoparticles (0.10 $\leq x \leq$ 0.50) it was shown that intentional oxidation by air exposure leads to an alumina film, which prevents further oxidation of the Cu bulk core.[21] From related metallurgical corrosion studies on NiAl, it is known that the particular oxidation conditions, i.e., temperature and oxygen pressure, have a large influence on the kinetics of Al diffusion and the formation of alumina on the NiAl surface.[5] In order to determine the minimum amount of Al which is necessary to prevent the oxidation of the Ni component, presumably by formation a fully developed shell around the remaining Ni/Al core of the particle, the above-described α-/β-Ni$_{1-x}$Al$_x$ powder samples (0.09 $\leq x \leq$ 0.50) were oxidized by careful exposure to oxygen at room temperature. The vials containing the highly oxophilic samples were left

open in the glovebox over night (O$_2$ $\sim$ 1 ppm in Ar), then taken out and left standing open in air for 24 h.

Characterization. In the XRD diagram of the β-Ni$_{0.50}$Al$_{0.50}$ sample (NP1) after air oxidation (Figure 11a, top) the reflections became broader and a loss of intensity was observed, indicating a deformation of the β-NiAl structure. The XRD pattern of α-Ni$_{1-x}$Al$_x$ powder samples (0.09 $\leq x$ $\leq$ 0.33) after air oxidation (Figure 11, parts c and d, top diagrams) exhibit no changes in comparison to the samples under argon.

The oxidized powder samples were annealed at 1000 °C in a sealed quartz ampule in vacuo to determine the presence of NiO (mp 1985 °C), i.e., to find out which sample has an insufficient Al content for a full alumina shell. However, in all cases, only reflections of Ni were observed (Figure 11 bottom diagrams). This indicates that even at a low Al content of 9 atom % in the alloy, air-stable Ni particles are obtained. The reflections of α-Al$_2$O$_3$ (corundum, JCPDS no. 46-1212) appeared as very weak, broad 2θ signals at 26°, 36°, and 67°. With decreasing Al content ($x < 0.17$), the reflections were not visible any longer. These findings show that XRD does not give a sufficient proof for the absence of any NiO in the bulk particle core. In order to re-evaluate the XRD results and analyze the particle composition after oxidation in more detail, particularly the oxidation state of nickel, XPS measurements on the air-oxidized β-Ni$_{0.50}$Al$_{0.50}$ sample (25 °C) were carried out. Additionally, the oxidation of all synthesized Ni$_{1-x}$Al$_x$ (0.09 $\leq x \leq$ 0.50) particles was investigated by XAS.

XPS Measurements. Numerous groups have studied the surface oxidation process in NiAl alloys with XPS;[4a,49–51] however, in most cases, typically thin film samples were preheated (>1000 °C) in ultrahigh vacuum and then treated with oxygen gas, usually below 10^{-5} mbar. In all these reports, the selective Al oxidation to alumina was observed, with Ni still being in the zero-valent oxidation state, which may give rise to softer oxidation processes. In the case of exposure to ambient air at atmospheric pressure, the conditions of oxidation, especially of small particles with a high surface, are much different. The groups of Young et al.[50] and Venezia et al.[51] studied the oxidation behavior of Ni$_{0.50}$-Al$_{0.50}$ and γ'-Ni$_3$Al, respectively, at atmospheric pressure conditions (>700 °C) by XPS. Before oxidation, a strong Ni 3p signal was observed at 66.8 eV, characterizing the clean alloy. Accordingly, the Al 2p$_{3/2}$ signal of alloyed Al at 72.9 eV was clearly visible. The Ni 2p$_{3/2}$ signal was visible at 853.0 eV, accompanied by a d^9 satellite at around 859 eV. It was found that upon oxidation the Al signal shifted to 76.0 eV and the Ni 3p peak lost intensity and moved to 70.0 eV, thus arguing that the surface of oxidized NiAl consisted of a top layer of NiO, with a mixture of Al$_2$O$_3$ and NiAl$_2$O$_4$ below. This work correlates with the earlier

(48) Ma, Y.; Du, Y. *J. Alloys Compd.* **2005**, *395*, 277–279.

(49) (a) Arranz, A.; Palacio, C. *Langmuir* **2002**, *18*, 1695–1701. (b) Bardi, U.; Atrei, A.; Rovida, G. *Surf. Sci.* **1992**, *268*, 87–97.
(50) (a) Young, E. W. A.; Rivière, J. C.; Welch, L. S. *Appl. Surf. Sci.* **1987**, *28*, 71–84. (b) Young, E. W. A.; Rivière, J. C.; Welch, L. S. *Appl. Surf. Sci.* **1988**, *31*, 370–374.
(51) (a) Venezia, A. M.; Loxton, C. M. *Surf. Interface Anal.* **1988**, *11*, 287–290. (b) Venezia, A. M.; Loxton, C. M. *Surf. Sci.* **1988**, *194*, 136–148.

Table 2. Deviation of the 2θ XRD Reflections from the Ni fcc Structure in Dependence of the Atomic Al Content (Determined by Elemental Analysis) and the Lattice Plane Constants of the Synthesized α-Ni$_{1-x}$Al$_x$ Phases

	$2\theta_{Lit}$ [deg][a]	$\Delta 2\theta$ [deg]			
$h\,k\,l$	Ni	$x = 0.082$	$x = 0.170$	$x = 0.253$	$x = 0.341$
(1 1 1)	44.508	0.084	0.087	0.087	0.088
(2 0 0)	51.847	0.169	0.234	0.448	0.970
(2 2 0)	76.372	0.097	0.166	0.360	0.526
(3 1 1)	92.947	0.191	0.217	0.446	1.057
(2 2 2)	98.449	0.212	0.284	0.561	1.407
d_{220} [Å][b]	2.4939	$2.4968 \pm 3 \times 10^{-4}$	$2.4996 \pm 3 \times 10^{-4}$	$2.5049 \pm 3 \times 10^{-4}$	$2.5096 \pm 3 \times 10^{-4}$

[a] Data taken from the JCPDS database no. 4-0850. [b] Calculated with the Bragg equation (Cu Kα radiation; λ = 1.54178 Å).
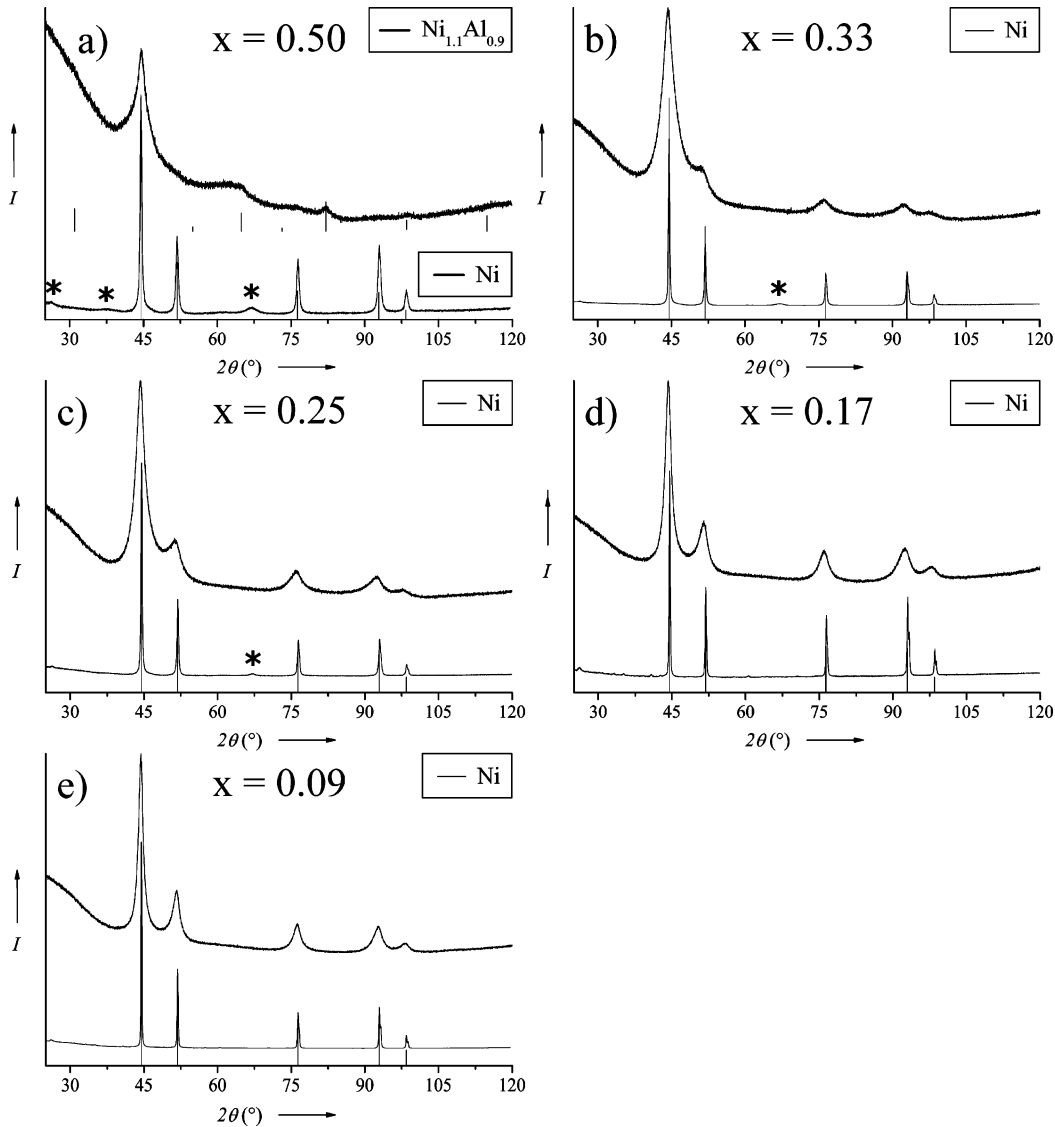

Figure 11. XRD diagrams of powder nanoparticles of (a) Ni$_{0.50}$Al$_{0.50}$, (b) Ni$_{0.67}$Al$_{0.33}$, (c) Ni$_{0.75}$Al$_{0.25}$, (d) Ni$_{0.83}$Al$_{0.17}$, and (e) Ni$_{0.91}$Al$_{0.09}$ phases, after air oxidation (top diagrams) and after annealing in sealed quartz ampoules at 1000 °C in vacuo (bottom diagrams). The asterisks mark the reflections of α-Al$_2$O$_3$.

work of Kuenzly and Douglass on the air oxidation of Ni$_{0.50}$-Al$_{0.50}$ at *T* > 900 °C, giving a mixture of NiO, NiAl$_2$O$_4$, and Al$_2$O$_3$, shown by XRD.[52] If the pressure was, however, lowered (e.g., 10^{-7} mbar), no Ni^{2+} species could be found.[51] These findings of Young and Venezia are in qualitative agreement to our observed X-ray photoelectron spectrum of the oxidized NP1 nanoparticles, shown in Figure 12. In the close-up spectra of the Ni region, besides the peak of the Ni

2p$_{3/2}$ photoelectrons at 856.7 eV, a shake-up satellite, characteristic for NiO, appeared at 862.0 eV, pointing at oxidized Ni on the particle surface. The Al region shows the signal of Al 2p$_{1/2}$ at 74.5 eV and a very weak Ni 3p peak at 68.1 eV. For this reason, in all other α-Ni$_{1-x}$Al$_x$ samples (*x* < 0.50), NiO would have been observed by XPS, and thus, there was no reason to perform further studies on those samples, too. Although NiO was detected, XPS only describes the situation at the particle surface, and it is still unclear whether Ni is also oxidized in the bulk core.
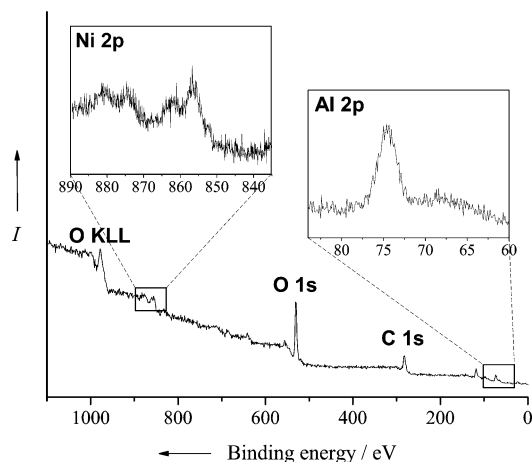
(52) Kuenzly, J. D.; Douglass, D. L. *Oxid. Met.* **1974**, *8*, 139–178.

Figure 12. XPS overview spectrum of oxidized $Ni_{0.50}Al_{0.50}$ nanopowder NP1. The Ni (left) and Al region (right) spectra are shown as insets.
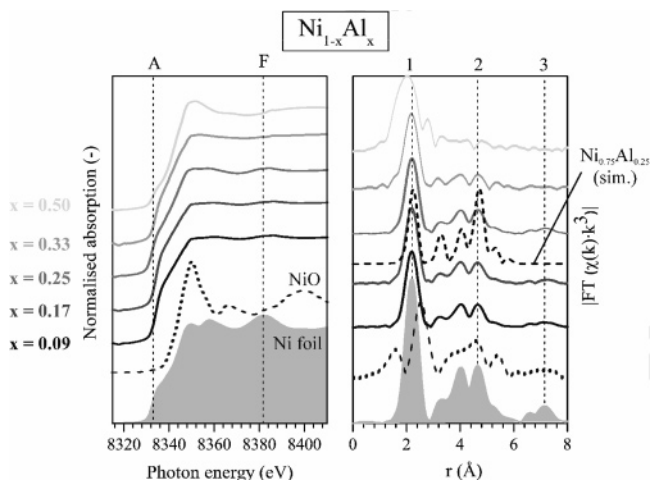

Figure 13. XANES (left) and EXAFS (right) of $Ni_{1-x}Al_x$ samples after oxidation. For comparison, the FT of a simulated $Ni_{0.75}Al_{0.25}$ FT has been added (thin closed line, EXAFS, right).

XAS Studies. The local structure around the central nickel atom was examined by XAS at the Ni K edge (8333.0 eV). The samples were deliberately oxidized prior to measurement, in order to establish the role of a protective layer around the core. In Figure 13, the X-ray absorption near-edge spectra (XANES, left) and the extended X-ray absorption fine structure spectra (EXAFS, right) of samples and reference materials are shown. The edge position (see XANES) of the samples is similar to that of metallic nickel (dashed curve) and clearly different to that of NiO (dash–dot curve). Thus, the XANES show that the nickel has not been oxidized as a result of the treatment and is indeed protected by a closed shell.

Alloy formation evidence obtained from XAS has been documented by several authors.[53–56] The XANES spectra for NiAl alloys reported in this literature appear to show rather substantial differences, which is likely due to the particle

size of the samples used. Smaller, often disordered particles can lead to less pronounced features in the XANES.[56] The analysis of the Ni K edge spectra is further complicated by the fact that similarity exists between spectra of Ni foil and Raney nickel.[53] In the nomenclature of ref 53, feature F in the XANES is indicative of a Ni−Ni resonance scattering found only in the metal and could serve as a fingerprint to distinguish the alloy from the metal. In our samples, this feature was found in the spectra of $Ni_{0.75}Al_{0.25}$, $Ni_{0.83}Al_{0.17}$, and $Ni_{0.91}Al_{0.09}$, but it is absent in the case of $Ni_{67}Al_{33}$ and $Ni_{50}Al_{50}$. This suggests that for these three samples, Ni is present in its fcc lattice matching the XRD data. In the Fourier transform, a substantial incorporation of aluminum into the Ni lattice ($Ni_{50}Al_{50}$) leads to a splitting of the first peak as reported in refs 53−55. In our samples, a splitting is only seen in the case of the β-NiAl particles. Modeling of this spectrum with FEFF paths generated from model NiAl compounds proved unsuccessful due to the poor data quality, likely due to the coexistence of several Ni-containing phases. This observation is further substantiated by the absence of higher shells, suggesting the lack of long-range order. In our opinion, the argument of whether nickel metal or alloyed NiAl is present is settled by the appearance of the χ-function (see the Supporting Information). Clearly, the sample denoted as $Ni_{0.75}Al_{0.25}$ is similar to the Ni reference foil, confirming the XRD data (vide supra), whereas the *simulated* spectra of Ni foil and a $Ni_{0.75}Al_{0.25}$ alloy show obvious differences. The higher shells in the EXAFS (see peaks labeled 2 and 3) are visible for samples which contain more Ni ($Ni_{1-x}Al_x$, $x < 0.33$). These higher shells also coincide with the higher shells of fcc-nickel. The small intensity of the first peak in the FT for the $Ni_{1-x}Al_x$ ($x < 0.33$) samples is not fully understood. Higher shells are evident in these samples (see Figure 13), which suggests more long-range order, and thus larger particles. A coexistence of smaller and larger particles is not excluded by the TEM images. Incorporation of Al into the Ni lattice without consequent splitting of the first peak is also considered. The first FT peak would then be broadened and reduced in height. In light of the presence of feature F in the XANES, we tend to exclude the latter explanation.

Conclusion

In summary, we presented a novel versatile, soft chemical approach to NiAl nanoparticles with a freely adjustable Ni/Al ratio. Two precursors for the Al component were successfully employed, namely, $[(Me_3N)AlH_3]$ and $[(AlCp^*)_4]$, which were combined with $[Ni(cod)_2]$ to yield the respective α-/β-NiAl phases. The particles remain largely unaffected against exposure to ambient air, due to the formation of an alumina layer, which is obviously formed in situ by diffusion of Al to the particle surface. The Ni-rich core is thus protected against further oxidation as expected from classical metallurgical data on NiAl alloys and matching known thin film surface chemistry of single-crystalline β-NiAl. However, a rigorous exclusion of any oxidation (oxygen getter effects) has not been possible with our experimental approach. The primary β-NiAl nanoparticles derived using $[(AlCp^*)_4]$ form metastable colloids in solution.

(53) Modrow, H.; Rahman, M. O.; Richards, R.; Hormes, J.; Bönnemann, H. *J. Phys. Chem. B* **2003**, *107*, 12221−12226.

(54) Arčon, I.; Mozetic, M.; Kodre, A.; Jagielski, J.; Traverse, A. *J. Synchrotron Radiat.* **2001**, *8*, 493−495.

(55) Balasubramanian, M.; Pease, D. M.; Budnick, J. I.; Manzur, T.; Brewe, D. L. *Phys. Rev. B: Condens. Matter Mater. Phys.* **1995**, *51*, 8102−8106.

(56) Tkachenko, O. P.; Klementiev, K. V.; van den Berg, M. W. E.; Gies, H.; Grünert, W. *Phys. Chem. Chem. Phys.* **2006**, *8*, 1539−1549.

The alternative Al source, [(Me₃N)AlH₃], is also a valuable precursor for the synthesis of nanoscaled metal aluminide alloys. However, the use of [(Me₃N)AlH₃] does so far not allow the preparation of colloidal metal aluminide nanoparticles. The reaction of the alane with [Ni(cod)₂] is very vigorous and rapidly leads to the precipitation of a nanocrystalline NiAl powder material. The advantage of the alane over [(AlCp*)₄] is the better synthetic availability. Whereas [(Me₃N)AlH₃] can easily be synthesized in mass scales of 20 g by a simple salt metathesis reaction from Me₃NHCl + LiAlH₄,[26] the Al(I) compound is synthesized in four reaction steps, including the synthetically delicate reduction of Al(III) to Al(I) by the Na/K alloy.[25] However, the alane is highly reactive and the reaction very vigorous and uncontrolled and rapidly leads to the precipitation of a nanocrystalline NiAl powder material. Contrasting this, the sparingly soluble compound [(AlCp*)₄] is a mild reagent, which first has to be dissolved (>100 °C), before it decomposes to Al(0) under H₂ pressure. This causes an intrinsic delay of decomposition so that the time scale of releasing Al(0) matches quite well to that of the metal precursors used here.

It appears that [(AlCp*)₄] is an excellent choice for the wet nanometallurgy of aluminides, particularly when aiming at the stabilization of free-standing surface-protected metal aluminide nanoparticles. In order to further explain this, we speculate that at some intermediate stage of the formation of the NiAl particles, still intact [(AlCp*)₄] may bind to the particle surface, i.e., $(Cp*Al)_x@Ni_1Al_{1-x}$ in a way being comparable to the known molecular cluster chemistry of species such as [Ni(AlCp*)₄] and other [Mₐ(AlCp*)ᵦ]. In that latter cases the AlCp* moiety acting as very strong σ-donor ligand to the zero-valent transition metal centers.[31−33,57] Prolonged hydrogenolysis at elevated temperatures completely splits the remaining Cp* group from the Al centers and/or from the aluminide nanoparticles in the form of Cp*H. It should be noted here that we have described unsaturated reactive species [M(AlCp*)ₙ] (n = 4 and M = Fe, Ru; n = 3 and M = Ni) which activate small molecules and in particular also C−H bonds from the Cp* ligand.[32,57] Due to the above-described catalytic properties of the NiAl surface, some hydrogenation of the Cp*H and further coupling reactions of still unsaturated products may take place which eventually leads to the above-mentioned formation of oligomeric hydrocarbon species, which act as primary protection against agglomeration. This poorly defined primary shell is, however, easily replaced by ACA. The acid strongly binds to the particle surface—at this stage being presumably only partly oxidized—and thus greatly enhances the stability of the colloidal solution.

Our results suggest that the ACA-stabilized NiAl nanoparticles could be an attractive air-stable magnetic material and may serve as a model case for subsequent and related studies. We suggest to protect extremely air-sensitive magnetic nanoparticles derived from the controlled hydrogenolysis of organometallic precursors, e.g., Fe, Co, or important binary alloy phases, such as CoRh, by *doping* the particles with small amounts of aluminum via the use of [(AlCp*)₄] and then use subsequent gentle oxidation to generate the desired alumina@metal core−shell structure with a controlled alumina thickness. The protection of magnetic metal nanoparticles with dielectric oxide layers allowing further processing has been identified as an important direction of nanoparticle research.[58]

Supporting Information Available: Figures of the IR spectrum of the β-NiAl nanoparticles NP1, the ¹H NMR spectra of the test of the catalytic activity of the β-NiAl colloids NP3 (before and after hydrogenation of cyclohexene), as well as the figure of the estimation of the Al content in the ACA@NiAl nanoparticles via Vegard's law (PDF). This material is available free of charge via the Internet at http://pubs.acs.org.

CM071411I

(57) Steinke, T.; Cokoja, M.; Gemel, C.; Kempter, A.; Krapp, A.; Frenking, G.; Zenneck, U.; Fischer, R. A. *Angew. Chem., Int. Ed.* **2005**, *44*, 2943−2946.

(58) Lu, A.-H.; Salabas, E. L.; Schüth, F. *Angew. Chem., Int. Ed.* **2007**, *46*, 1222−1244.